RSC Advances

ROYAL SOCIETY OF CHEMISTRY

www.rsc.org/advances

Synthesis of α-$Fe_{2-x}Ag_xO_3$ Nanocrystals and Study of their Optical, Magnetic and Antibacterial properties

Mayank Bhushan,[a] S. Muthukamalam,[b] S. Sudharani,[b] Annamraju Kasi Viswanath[*,a]

[a] Centre for Nanoscience and Technology, Pondicherry University, Puducherry - 605014, India.

[b] Department of Biochemistry and Molecular Biology, Pondicherry University, Puducherry - 605014, India.

[*] v_kasi@hotmail.com

Abstract:

To be an implicit disinfectant, the inorganic nanoparticles have to show chemical stability, minimum cytotoxicity and effective bactericidal activity. Among metal oxide nanoparticles, iron oxide demonstrate a very high structural stability in corrosive biological environment and also have relatively non-toxic profile in comparison with other metal nanoparticles such as ZnO. Iron oxide nanoparticles also exhibit bacterial growth inhibition property on a wide spectrum of bacterial species mainly by generating reactive oxygen species (ROS) from water and oxygen. However, the efficiency of their antibacterial activity remains less. Probably, the main reason behind it is aggregation and occurrence of large flocculates of nanoparticles in an aqueous media due to their hydrophobic nature and hence their interaction with bacteria is limited. To overcome all these problems, in this study we incorporate silver ions into α-Fe_2O_3 to produce magnetic hybrid nanostructures with better colloidal stability and enhanced antibacterial activity due to their synergistic effect. The antibacterial activity of prepared nanospheres was tested at 3 different concentrations (450, 600, 750 µg) against four bacterial strains - *Bacillus subtilis, Staphylococcus aureus, Pseudomonas fluorescens* and *Escherichia coli* by disc diffusion method. The nanospheres showed concentration dependent activity profile and remarkably, they were very effective against *B. subtilis* and *P. fluorescens*. Their antibacterial effect was found to be comparable to the standard antibiotic streptomycin used in this study. Furthermore, in this work structural, optical and magnetic properties of prepared samples have been studied using different characterization tools.

Keywords: α-Fe_2O_3 nanoparticles, Ferromagnetism, antibacterial activity, Optical and Magnetic property.

1. INTRODUCTION

On a large scale, the evolution of nanotechnology has started with semiconductor industry due to a continuous demand of low dimensional materials with better electrical and optical properties for device fabrication.[1-5] Because of their extremely small size range, nanomaterials exhibit a wide variation in their physical, chemical and physiological properties compare to their bulk counterparts. And here lies the opportunity to tune the properties of nanoparticles based on our requirement. Antibacterial materials play an important role in maintaining human health care by providing efficient treatment for the infectious diseases caused by pathogenic bacteria.[6,7] Considering a wide range of antibacterial agents available today, silver based

nanomaterials have got large attention due to their high throughput and wide spectrum bactericidal activity.[8-10] These inorganic nanostructures have distinct advantage over conventional chemical bactericides as they suffer through multidrug resistance. In general, the bactericidal property of chemical agents relies on their specific binding with microbial cell wall or, surface and metabolism of agents into the micro-organism. A range of pathogenic micro-organisms have evolved drug resistance during course of time over many generations. So far, these chemical based conventional antimicrobial agents have been effective for therapy; however, their use has been confined to medical instruments and in prophylaxis in antimicrobial facilities. Hence, to find an unorthodox way to overcome the drug resistance of wide range of pathogenic microorganisms is very much needed on urgent basis. Silver ions and silver salts have been known for their growth-inhibitory property against microorganisms and have been used for the same in past. Also, activity of other metal ions like Cu,[11,12] Zn[13,14] and Mg[15] against microorganisms have been reported by various research groups. However the usefulness of Ag ions or salts as such as an antimicrobial agent has got some limitations due to various reasons, including the restraining effects of salts. In sharp contrast, these kinds of shortcomings can be overcome by the use of Ag nanoparticles which produce enhanced antimicrobial property in comparison with the bulk. The mechanism behind this high bactericidal activity is that silver cations, i.e., Ag^+ ions could damage the bacteria by binding with the thiol groups of proteins and also by interrupting with DNA replication mechanism which leads to loss of DNA replication ability of bacteria and hence eventually causes death of bacteria.[16,17] In addition, antibacterial behavior of silver has also been reported specifically due to inactivation of enzyme phosphomannose isomerase.[18] Therefore high throughput of antibacterial activity of silver based compounds mainly depends on controlled and durable generation of Ag^+ ions. There are few limitations which restrict the use of silver salt and silver nanoparticles, constituents of a number of commercial bactericidal products, in their further application in many areas.[19] The main reason behind this is abrupt release of Ag^+ ions from the silver salt, causing potential danger for human life and environmental safety. The applications of Ag nanoparticles are also limited by occurrence of large aggregations and murky Ag^+ ions release, resulting into loss of antibacterial activity.[20] To solve the issues mentioned above, integration or, innovation of nanostructured silver based nanomaterials with prolonged and efficient bactericidal activity is the need of hour. So, to use bactericidal property of Ag in various fields against pathogenic and drug resistant microorganisms, it is essentially required to prepare the Ag based systems with cost-effective methods and also to know the mechanism involved in causing the antimicrobial effect. Also, it is very much crucial to intensify the antimicrobial effect. Antibacterial properties of α-Fe_2O_3 nanoparticles and their composites on different bacteria have been reported by few groups[21-23] and also antibacterial studies of Ag@Fe_3O_4 and **γ**-Fe_2O_3@Ag has been reported by R. Prucek et al.[24] Recently, antibacterial properties of iron oxide @ carbon nanocomposites have been reported against *E.coli* and *S. aureus.*[25,26] In this study we report the cost-effective preparation of Ag doped α-Fe_2O_3 homogeneous and stable nanoparticles. The nanosize of the hybrid system has provided enhanced surface area with the microorganisms, and also due to its nanoscale size it can easily be applied to medical devices using surface coating methods.

Study of magnetic properties of nanostructures has drawn significant scientific surveillance due to their multi-disciplinary prospective applications such as in biotechnology,[27-30] electronics, magnetic fluids, catalysis, memory devices[31] and environmental treatment. Recently, various groups have worked on detection of bacterial pathogens (*Pseudomonas aeruginosa*)[32] and viral pathogens like hepatitis B[33,34] and porcine endogenous retrovirus (PERV)[35] based on magnetic properties of iron oxide nanoparticles and chemiluminescence. Also, these properties have been used to develop an analytical system to analyze copy number variation of DNA.[36] To accomplish these applications, different approaches have been used for preparing magnetic nanocomposites with many distinct

compositions.[37-40] As iron oxide nanoparticles exhibit minimum level of cytotoxicity compared with other metal oxide nanoparticles,[41] along with drug carrier and MRI contrast agent they have also been used for detecting overexpression of cyclooxygenase-2 (COX-2) and B-cell lymphoma-2 (BCL-2) associated with gastric cancer.[42,43] Iron oxide (α-Fe_2O_3) nanomaterials exhibit a classic rhombohedral crystal structure and are preferred while preparing magnetic hybrid nanocomposites because of their inherent magnetic properties associated with the nanoscale size and surface effects. The Fe_xO_y nanomaterials are generally susceptible to high magnetic response in presence of an externally enforced magnetic field and hence possess a potential use in recyclable nanocatalysis, selective capturing of intended substrates and magneto-photonic purposes.[44-50] Here, in this work, we report the synthesis of α-$Fe_{2-x}Ag_xO_3$ systems for the first time which is Ag doped hematite nanostructures through chemical co-precipitation method and study of their structural, optical, magnetic and antibacterial properties against four different bacterial species (both gram positive and gram negative).

2. Materials and Methods

2.1. Materials

Ferrous Sulphate ($FeSO_4.7H_2O$), Silver Nitrate ($AgNO_3$), Sodium Hydroxide (NaOH) and Sodium Dodecyl Sulphate (SDS) were purchased from Sigma Aldrich, India. Ethanol, nutrient broth and nutrient agar media were purchased from Hi-media, India.

2.2. Preparation of nanoparticles

Ferrous sulphate heptahydrate (0.1 M) and respective weight of $AgNO_3$ corresponding to 1, 3, 5 and 7 atomic weight % of Ferrous sulphate heptahydrate were dissolved in 100 ml of double distilled water in four different beakers (250 ml) and allowed for proper mixing for 2 hrs by stirring using a magnetic stirrer. After that 1% wt./vol. of SDS was added to all the beakers and allowed for stirring for 1 hr. followed by addition of 50 ml of NaOH solution (0.4 M) drop wise in all the beakers under continuous stirring. All the solutions were kept for overnight stirring and then washed thrice with double distilled water and once with ethanol using ultracentrifugation operated at 800 rpm for 10 minutes each time. The resulting samples were dried in hot air oven at 32°C for 1 hr and used for further characterization after annealing at 800°C for 3 hrs. One more sample was prepared by adopting same procedure but without adding $AgNO_3$. Details and name of all the samples is given in table 1.

Table 1: Samples code and composition

S.N.	Sample Code	Composition	Atomic wt% of Ag	%wt/vol of SDS used for synthesis
1.	IS	α-Fe_2O_3	0	1
2.	ISS1	α-$Fe_{1.99}Ag_{0.01}O_3$	1	1
3.	ISS2	α-$Fe_{1.97}Ag_{0.03}O_3$	3	1
4.	ISS3	α-$Fe_{1.95}Ag_{0.05}O_3$	5	1
5.	ISS4	α-$Fe_{1.93}Ag_{0.07}O_3$	7	1

2.3. Characterization

The prepared samples were used to study the structural events using Rigaku Ultima IV X-ray Diffractometer with Cu K_α=1.5418A^o , operating voltage 40kV, current 40mA and step size 0.02^o in 2θ scan. SEM micrographs were recorded by Hitachi, Model S-3400N equipped with Energy dispersive spectroscope. The Raman spectra were obtained with Confocal-Raman spectrometer excited by Ar^+ laser 488 nm lines. The Thermo NicoletModel6700 Fourier transform infrared spectroscopy (FTIR) was used to confirm the chemical bonds and the nature of the sample. Perkin Elmer λ_{650} UV-Visible spectrophotometer was used for UV-Visible absorbance spectrum. Thermal behavior of the sample was studied by Model Q600 SDT and Q20 DSC Thermo Gravimetric analysis (TG/DTA) and the magnetic properties were characterized by vibrating sample magnetometer VSM Lake Shore 7404 at room temperature. All the characterizations were done according to standard operational procedures.

2.4. Antibacterial activity of α-$Fe_{2-x}Ag_xO_3$ nanospheres

2.4.1. Growth Curve

Fresh bacterial colonies were inoculated in 100 ml of nutrient broth to study the bacterial growth in nutrient broth media. The test samples IS, ISS1, ISS2, ISS3 and ISS4 annealed at 800°C for 3 hrs were supplemented with the media in a concentration of 45 mg/dl, 60 mg/dl, 75 mg/dl, 90 mg/dl and 120 mg/dl. The bacterial culture was then incubated at 37±1 °C with continuous shaking at 200 rpm. The culture without test sample was used as control to compare the effect of Fe_2O_3 nanoparticles. The growth of bacteria in broth media was determined by measuring the optical density (OD) at λ = 600 nm at regular intervals of time for 24 hrs using UV-Vis Spectroscopy. The growth curve was plotted between optical density and incubation time.

2.4.2. Disc diffusion

The antibacterial activity of the samples IS, ISS1, ISS2, ISS3 and ISS4 was assayed by the Kirby-Bauer disc diffusion method.[51] To achieve the desired concentrations, all the test samples were prepared by mixing known weight of nanoparticles with 1ml of distilled water followed by sonication for 2 minutes for homogenous distribution of nanoparticles. Nutrient agar plates were prepared by pouring molten agar into Petri plates at 55°C and allowed to set. Subsequently the plates were inoculated with the cultures of *E. coli* (Gram-negative bacteria), *P. fluorescens* (Gram-negative bacteria), *B. subtilis* (Gram-positive bacteria) and *S. aureus* (Gram-positive bacteria). Sterile circular Whatman filter paper disks of size 6 mm were placed on the agar and loaded with varying concentration of nanomaterials 450, 600 and 750 µgs respectively. Disks loaded with water served as solvent control and streptomycin (300 µg) as positive control. The petri plates were then incubated for 24 hrs at 37±1°C and the zone of inhibition was measured by using antibiotic zone scale (Hi media) for all the samples. All experiments were repeated thrice.

3. Results and Discussion

3.1. XRD

XRD patterns of Ag doped and undoped nanosized α-Fe_2O_3 samples were obtained after calcining the as prepared products at 800°C for 3 hrs and can be seen in fig. 1. All the sharp and strong diffraction peaks present in fig. 1 can be assigned to α-Fe_2O_3 with a hexagonal structure which is well consistent with the values in literature (JCPDS No: 33-0664). There is no extra peak analogous to Ag, oxides of Ag related secondary and impurity phases evident from the XRD spectra, which may be referred to the embodiment of Ag ions into the Fe lattice site rather than interstitial ones. The average crystallite size of nanoparticles was calculated using Debye - Scherrer's[52] equation:

$$D = 0.9\lambda/\beta\cos\theta \qquad \ldots..(1)$$

Where D is the average crystallite size (in nm), λ is the wavelength of Cu K α (0.154 nm), β is the full width at half maximum intensity (FWHM) in radian and θ° is the Bragg angle (°). The details of the data obtained from XRD are given in table 2. XRD patterns of sample IS with JCPDS data are given in figure 1 of supplementary information.

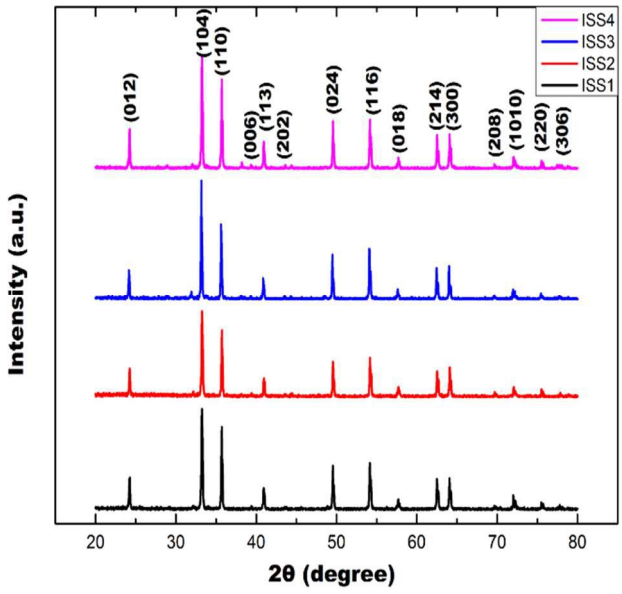

Fig.1. X-ray diffractograms of prepared Ag doped α-Fe_2O_3 nanospheres.

Table 2: The characteristic peaks of α-Fe_2O_3

Sample Code	Avg. Crystallite Size (nm)	2θ	Planes
IS	37.13	24.24	(012)
		33.27	(104)
		35.74	(110)
		40.93	(113)
ISS1	39.79	49.55	(024)
		54.17	(116)
ISS2	41.51	57.69	(018)
		62.52	(214)
ISS3	44.08	64.07	(300)
		69.64	(208)
ISS4	41.87	72.03	(1010)
		75.51	(220)
		77.78	(306)

3.2. UV-Vis Spectra:

The optical band gaps of all annealed samples were measured using UV-Vis absorption spectroscopic technique. The absorbance curves for all annealed samples are shown in figure 2 and it is clearly observed that the absorption maxima shifted from 534 nm to 570 nm as the silver content increases in the sample and also a slight decrease in intensity of absorption peaks has been observed with the increased silver content in the sample.

There are three explicit absorption regions present in the uv-vis absorption spectra of the undoped and Ag doped α-Fe_2O_3 nanoparticles. As per the references,[53,54] absorption between 250–400 nm primarily results from the ligand to metal charge-transfer transitions and slightly from the contribution of the Fe^{3+} ligand field transitions $^6A_1 \longrightarrow {}^4T_1$ (^4P) at 290–310 nm, $^6A_1 \longrightarrow {}^4E$ (4D) and $^6A_1 \longrightarrow {}^4T_2$ (^4D) at 360–380 nm. Absorption in the region between 400–600 nm is considered to arise due to the pair excitation processes $^6A_1 + {}^6A_1 \longrightarrow {}^4T_1$ (^4G) + $^4T_1$ (^4G) at 485–550 nm, probably imbricated the contributions of $^6A_1 \longrightarrow {}^4E$, $^4A_1$ (^4G) ligand field transitions at 430 nm and the charge-transfer band tail. Absorption in wavelength region between 600 – 800 nm is related to the $^6A_1 \longrightarrow {}^4T_2$ (^4G) transition at about 640 nm. However, the absorption intensity in regions between 250 - 400 nm and 400 - 600 nm is much larger than that in region between 600 - 800 nm, which implies that the absorption due to the charge-transfer transitions or the pair excitations is much stronger than the absorption due to the ligand field transitions because of the selection rules.

The optical band gap, E_g (for a direct transition between the valence and conduction band), was obtained from diffuse reflectance spectra by plotting the square of the product of Kubelka-Munk function $F(R)$ and energy as a function of energy. Kubelka-Munk function F(R) is estimated by using the relation

$$F(R) = (1 - R)^2 / 2R$$

Where, R is the magnitude of reflectance. Figure 3 shows the $(F(R)*E)^2$ as a function of energy for all undoped and Ag doped α-Fe_2O_3 samples annealed at 800°C and to obtain the optical band gap, the linear part of $(F(R)*E)^2$ curve was extrapolated until it intersects the energy axis at $(F(R)*E)^2 = 0$. The band gap for direct transition (estimated from figure 3) was found to be 2.28 ev, 2.81 ev, 2.91 ev, 2.93 ev and 2.96 ev for the annealed samples IS, ISS1, ISS2, ISS3 & ISS4 respectively. So, it clearly shows that the band gap energy increases with the increasing Ag content in the samples in comparison to undoped sample.

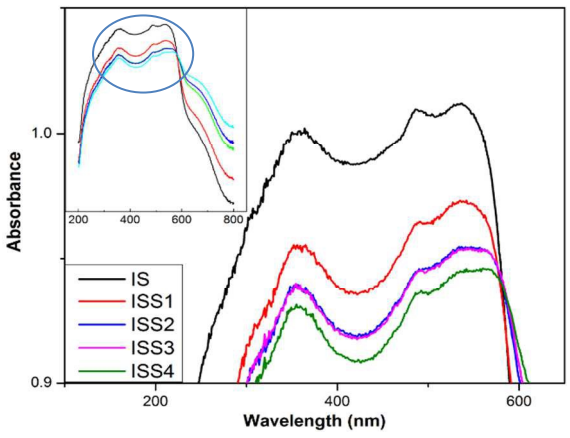

Fig. 2. UV-VIS absorption spectra for all the annealed samples.

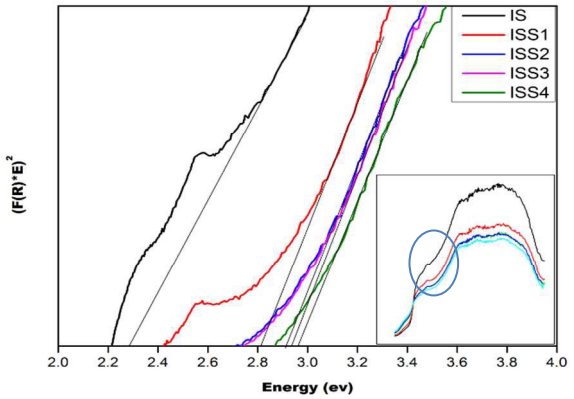

Fig. 3. The Kubelka-Munk Plots for all undoped and doped nano crystalline α-Fe_2O_3 powders.

3.3. Raman Spectrum:

The Raman spectra of undoped and Ag doped α-Fe_2O_3 samples annealed at 800°C for 3 hrs were taken and are shown in Fig. 4. The α-Fe_2O_3 with corundum-type crystal structure is the most common iron oxide on earth and seven phonon lines are expected to appear in the Raman spectrum, namely two A_{1g} modes (223 and 496 cm^{-1}) and five E_g modes (256, 292, 299, 408 and 607 cm^{-1}).[50] Our samples exhibit all the peaks corresponding to the typical frequencies observed for α-Fe_2O_3, as seen in the Raman spectra. However, some shifts were observed which may occur due to differences in size and shape of the particles. The sharp peak at around 1314 cm^{-1} is due to a two-magnon scattering which emerges from the correlation of two magnons created on antiparallel close spin sites.[55] The characteristic peaks at 666, 820, 1050 and 1103 cm^{-1} are observed only in highly crystallined hematite,[56] as our samples exhibit these peaks which again confirms the high crystalline nature of the prepared samples.

3.4. Thermal Analysis

Thermogravimetric (TGA) analysis and Differential Scanning Calorimetry (DSC) were executed for undoped and Ag doped α-Fe_2O_3 nanoparticles, to know the phase formation and decomposition which occurs in the course of heat treatment. The thermal analysis was carried out from room temperature to 800°C. TGA of as prepared samples was performed by heating in air atmosphere at 5°C/min in an alumina crucible. The DSC-TGA curve for the sample ISS2 is shown in Fig. 5 and TGA curves for all the samples are given in Fig. 2 of supplementary information. It is observed that the mass loss appears in a wide range of temperature from room temperature up to 660°C. The specific mass loss at temperatures below 100°C illustrates the existence of free water or physiosorbed water. Further, the extended downfall of relative mass versus temperature implies that the surface water molecules possibly remain in an immense set of energetically nonequivalent surface hydration groups. When the temperature is over to 640°C the sample mass eventually becomes constant. From the mass difference in TGA data, the total water content was determined to be as high as 27.51 wt.%. The downward peak in heat flow graph and further decrease of mass was observed at 248.8°C and 420.2°C in weight curve, which represent decompositions of $Fe(OH)_2$ and $Ag(OH)_2$ respectively. Both the materials liberate water molecules. The two exothermic peaks noticed in the DTA curve around 500 and 600°C are because of the burning of impurities. Beyond 640°C, a flatter weight loss curve is seen because of the release of water originating from the condensation reaction. These results were in good agreement with the literature.[57]

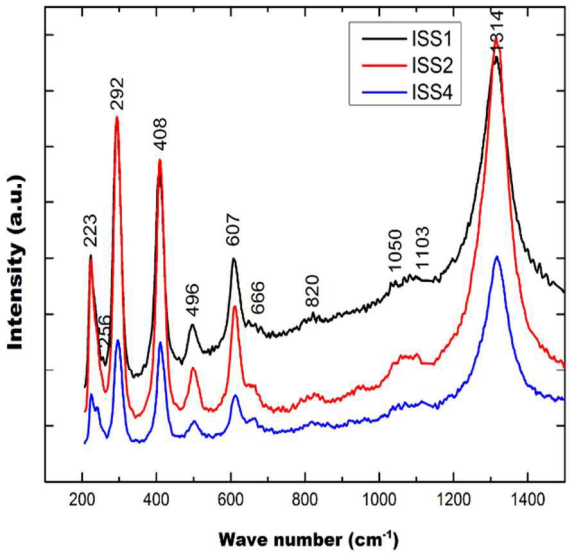

Fig. 4. Raman spectra of undoped and Ag doped α-Fe_2O_3 nanoparticles.

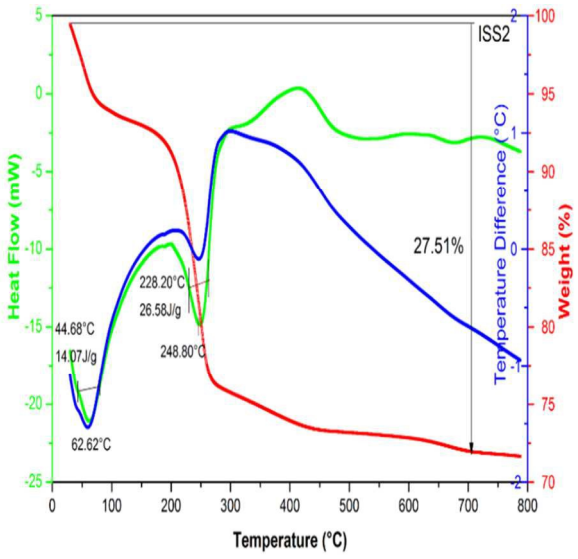

Fig. 5. DSC-TGA curve for sample ISS2.

3.5. VSM Analysis:

To study the magnetic behavior and the evolution of magnetism in pure and Ag doped α-Fe_2O_3 samples, measurements were made using a Vibrating Sample magnetometer at room temperature. Figure 6 shows the magnetic hysteresis loops of the annealed samples at various doping levels. α-Fe_2O_3 nanoparticles often exhibit the unusual magnetic behavior.[58] Presence of the free surface and grain boundaries leads to the improved magnetic properties.[59] The results demonstrate that they have weak ferromagnetic behavior. The saturation magnetization was not observed in the applied range of magnetization field. Table 3 shows the values of coercivity (H_c) and remanent magnetization (M_r). For samples ISS2 and ISS3, the values were almost approximate. However, the samples ISS1 and IS exhibited a higher value for M_r and shows strong hysteresis loop behavior. The ISS1 sample displayed the highest magnetic properties with M_r of 0.1672 emu/g and H_c of 1933 Oe. It must be due to the influence of Ag ion doping in hematite lattice. The variation of the magnetism with the increase of Ag-doping suggests that the crystallization quality of $Fe_{2-x}Ag_xO_3$ and the formation of the second phase also have great effect on the regular arrangement of the magnetic moment. Since the increase in Ag concentration is helpful to enhance the exchange interaction of the Ag ions between different bound magnetic polarons (BMP) areas, the ferromagnetism first increases with the increase of Ag-doping and then decreases. Therefore, the magnetization also has a doping dependent behavior for α-Fe_2O_3 samples.

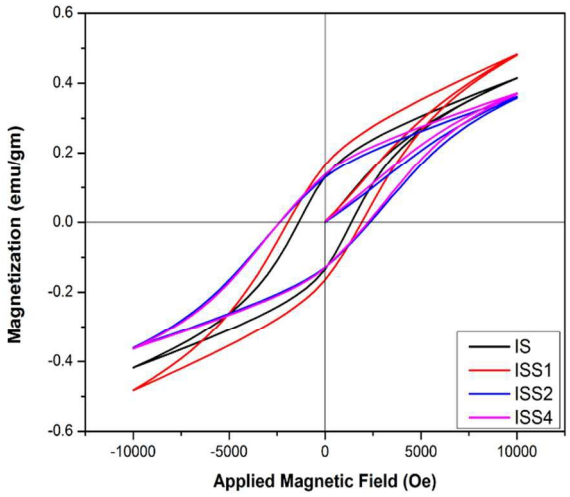

Fig. 6. B-H Curve of undoped and Ag doped α-Fe_2O_3 nanoparticles.

Table 3: Magnetic Parameters of Undoped and Ag doped α-Fe_2O_3 nanoparticles.

Sample Code	Coercivity (Gauss)	Retentivity (emu/gm.)*10^{-6}	Magnetization (emu/gm.)*10^{-3}
IS	1366.66	0.1344	0.4177
ISS1	1933.33	0.1672	0.4832
ISS2	2355.55	0.1298	0.3606
ISS4	2355.55	0.1403	0.3744

3.6. Scanning Electron Micrograph (SEM) and EDAX:

The size and morphology of all the annealed α-Fe_2O_3 samples were examined by SEM analysis. Figure 7 (a) shows the SEM image of sample ISS2, and it demonstrates that the nanoparticles have got agglomerated to some extent and possess almost spherical or, oval shape. Figure 7 (b) shows the EDS spot spectra of sample ISS2 (α-

$Fe_{1.97}Ag_{0.03}O_3$), showing the surface elemental components: Iron, Oxygen and Silver.

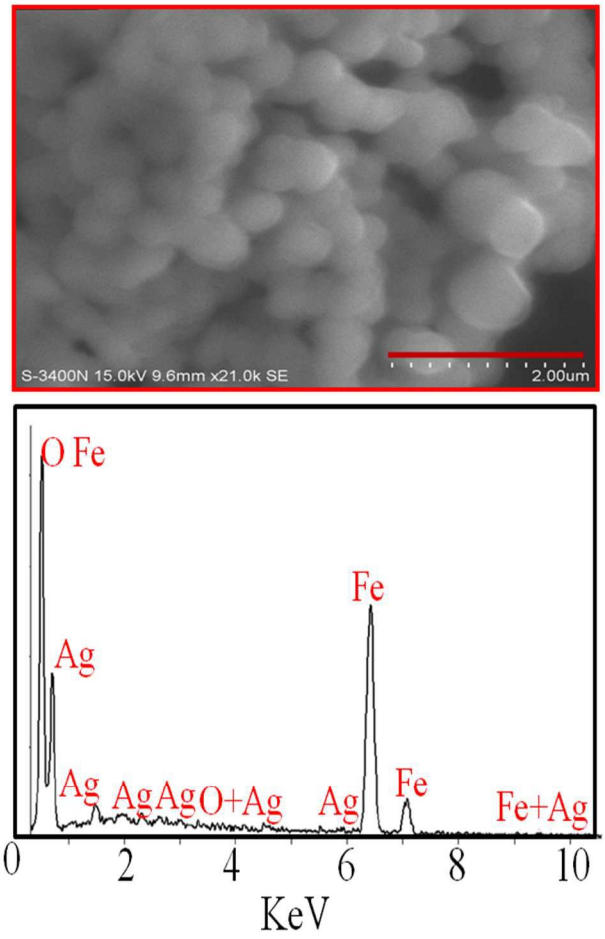

Fig. 7. (a) SEM image and (b) EDS spot spectra of sample ISS2 (α-$Fe_{1.97}Ag_{0.03}O_3$).

3.7. Analysis of antibacterial activity

The prepared undoped and doped Fe_2O_3 nanospheres are expected to exhibit antibacterial activity because of their robust Ag^+ ions release ability and also because of inherent native bactericidal property of hematite nanocrystals giving a synergistic effect in enhancing the bactericidal properties of hematite nanocrystals. The antibacterial activity of the samples ISS1, ISS2, ISS3, ISS4 and IS was assessed against four bacterial strains i.e., *E.coli*, *B. subtilis*, *P. fluorescens* and *S. aureus* by the disk diffusion method and the inhibition zones produced by them are shown in figure 8 (A-D). Figure for zone inhibition of sample IS against tested bacteria (8E) is given in supplementary information.

The principle of the Bauer-Kirby disc diffusion susceptibility test is to determine the sensitivity of pathogenic aerobic/facultative bacteria to various antimicrobial compounds. The paper disks impregnated with known concentrations of test compound when placed on agar plate, water is absorbed from the agar into the disks and the antimicrobial compound begins to diffuse into the surrounding agar. The presence or absence of growth around the disk is an indirect measure of the ability of that compound to inhibit that organism.

The results obtained in this study clearly indicated that diameter of inhibition zone depends upon the concentration of Fe_2O_3 nanospheres and as the concentration of nanospheres increases from 450 to 750 µg the inhibition zone diameter also increases. In our experiment, we have analyzed the effect of Ag doping in α-Fe_2O_3 nanospheres on the inhibition zone diameter by taking 450 µg, 600 µg and 750 µg from each of the IS, ISS1, ISS2, ISS3 and ISS4 samples respectively and got clear, significant and increasing inhibition zone with increasing concentration of the samples as well as with increasing Ag content in the samples, suggesting an effective antibacterial effect. The maximum inhibition zone was observed at concentrations of 600 & 750 µgs. The zone of inhibition produced by ISS3 & ISS4 against all the four bacterial strains used in this study was found to be equivalent and even improved as compared to the positive control streptomycin. The diameters of inhibition zone (in mm) for different concentrations of all the samples are tabulated in Table 4.

Furthermore, to establish the antibacterial effect of the nanomaterials, their effect on bacterial growth pattern against the *E. coli, B. subtilis*, *P. fluorescens* and *S. aureus* was monitored by measuring the optical density (OD) at 600 nm based on the turbidity of the cell suspension. The bacterial cultures were treated with five different concentrations 45 mg/dl, 60 mg/dl, 75 mg/dl, 90 mg/dl and 120 mg/dl of the samples ISS1, ISS2, ISS3, ISS4 and IS respectively and the OD values were recorded for 24 hrs at regular intervals of time and a graph was plotted between optical density and time as shown in figure 9 (A-D). Graph

between optical density and time for sample IS (fig. 9E) is given in supplementary information. The control flasks without treatment showed robust bacterial growth. On the other hand, reduced bacterial growth was observed in the presence of $Fe_{2-x}Ag_xO_3$ nanocrystals even at a concentration as low as 45 mg/dl. Interestingly, treatment with ISS3 & ISS4 at the concentration of 120 mg/dl resulted in complete growth inhibition in all the four bacterial strains used in this study (Fig. 9C and 9D). Similar effect was brought about by ISS1 and ISS2 with *P. fluorescens* (Fig. 9A and 9B). This observation clearly indicates that, as the concentration of undoped and doped Fe_2O_3 nanospheres increases the optical density decreased, measured bacterial growth was diminished whereas the control sample shows the growth rate increased with the time. From this analysis it was found that Fe_2O_3 nanospheres at 120 mg/dl concentration, show effective antibacterial property leading to no or very less bacterial growth. The minimum inhibitory concentration (MIC) varied with the samples. In the case of samples IS and ISS1 minimum inhibitory concentration was found to be 90 mg/dl against all the strains. The MIC value for sample ISS2 was found to be 75 mg/dl and for samples ISS3 and ISS4 the MIC value was 60 mg/dl against all the strains.

ISS1

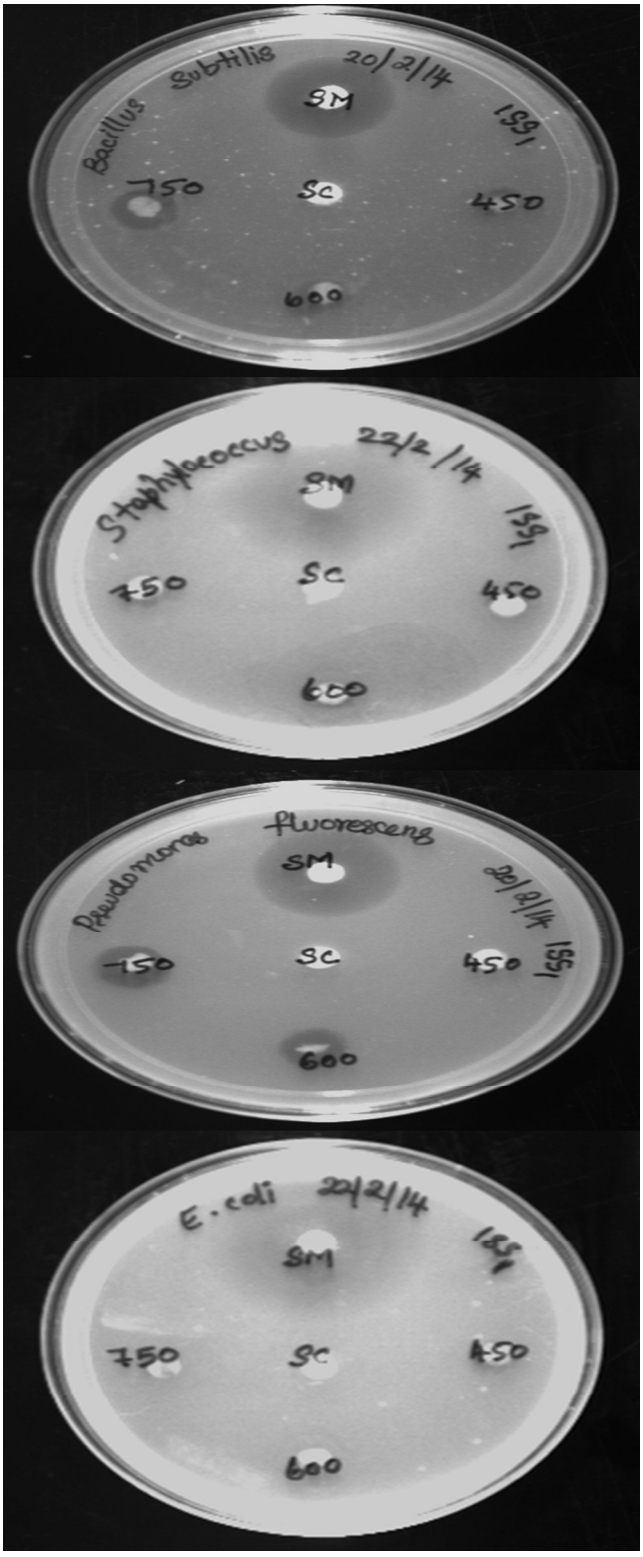

Fig. 8A: Zone inhibition of sample ISS1 against bacteria *B. subtilis*, *S. aureus*, *P. fluorescens* and *E. coli*.

ISS2

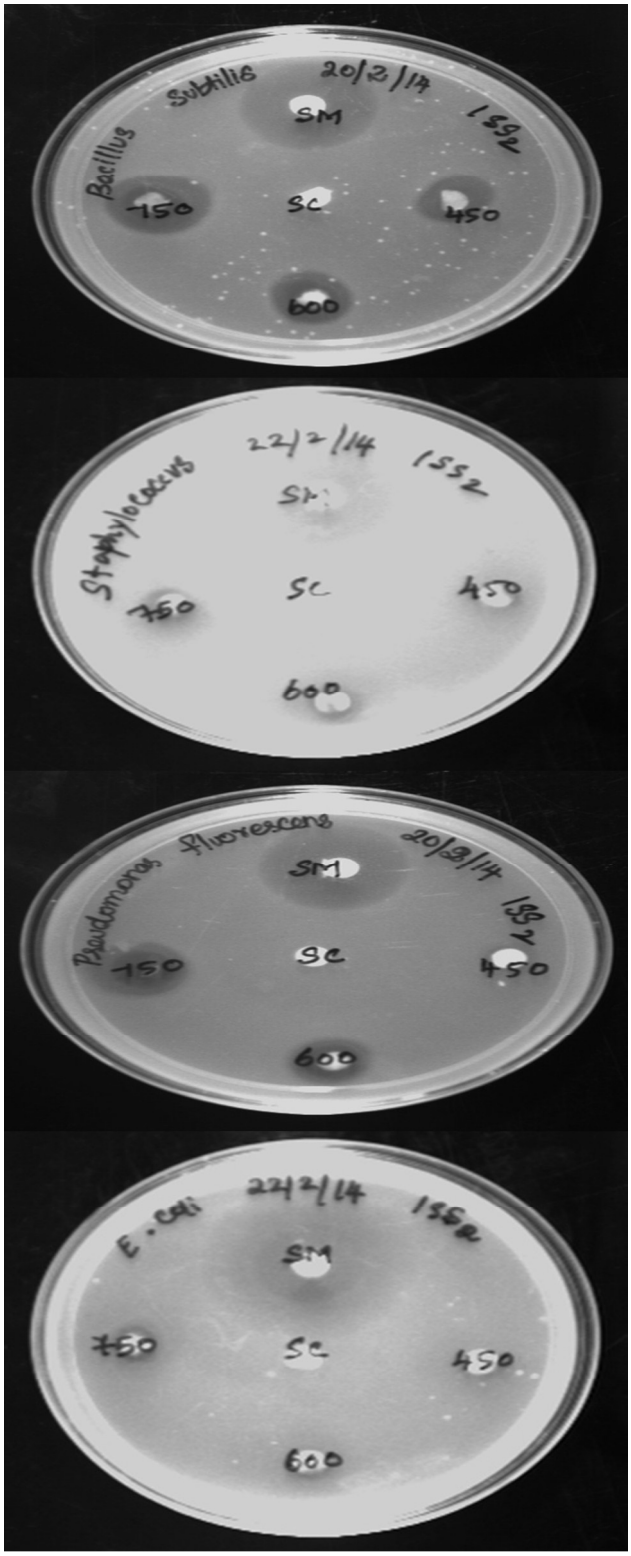

Fig. 8B: Zone inhibition of sample ISS2 against bacteria *B. subtilis*, *S. aureus*, *P. fluorescens* and *E. coli*.

ISS3

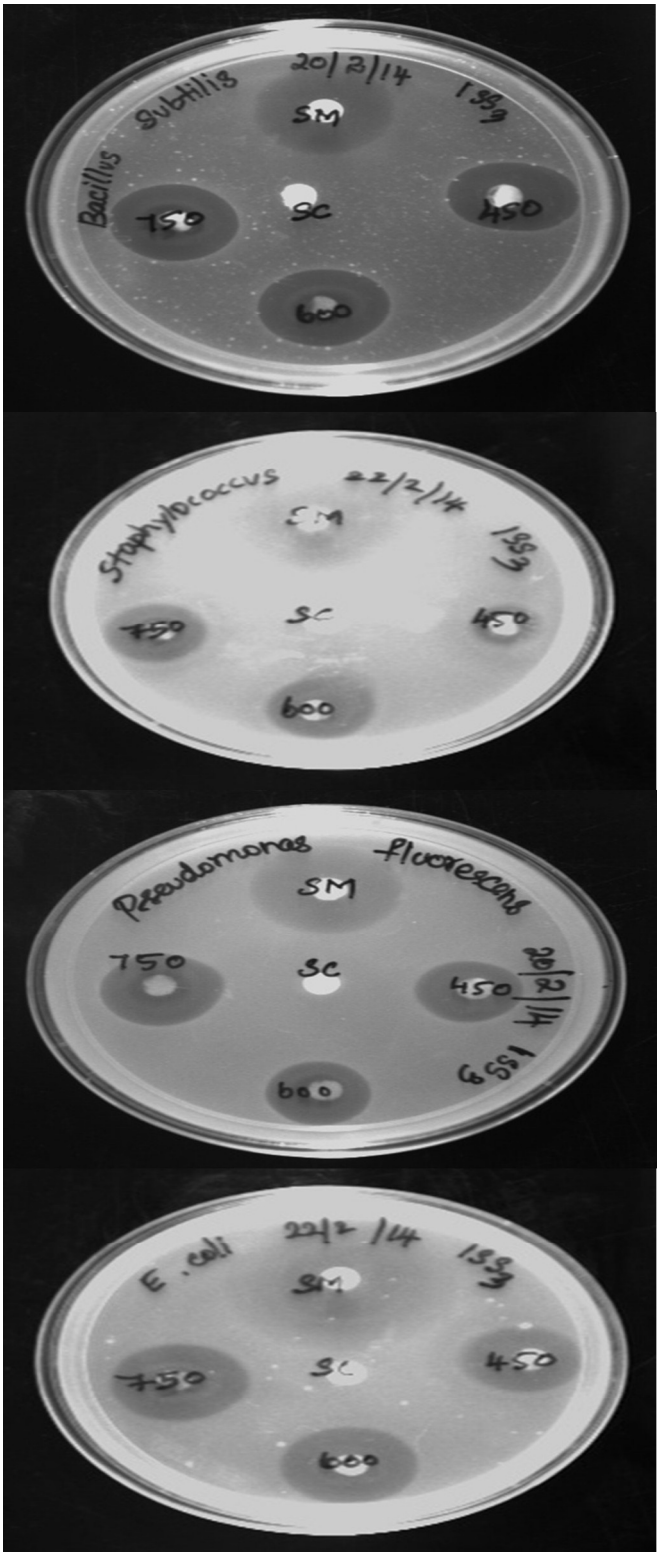

Fig. 8C: Zone inhibition of sample ISS3 against bacteria *B. subtilis*, *S. aureus*, *P. fluorescens* and *E. coli*.

ISS4

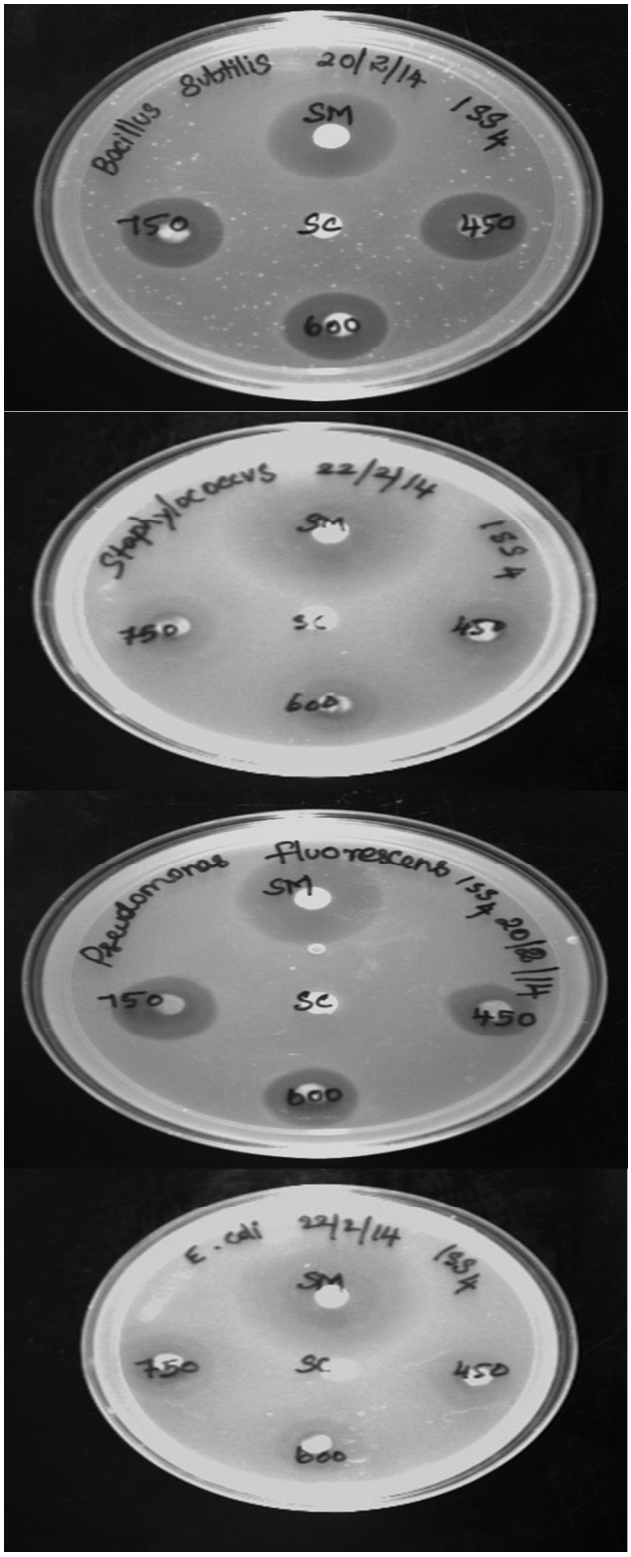

Fig. 8D: Zone inhibition of sample ISS4 against bacteria *B. subtilis*, *S. aureus*, *P. fluorescens* and *E. coli*.

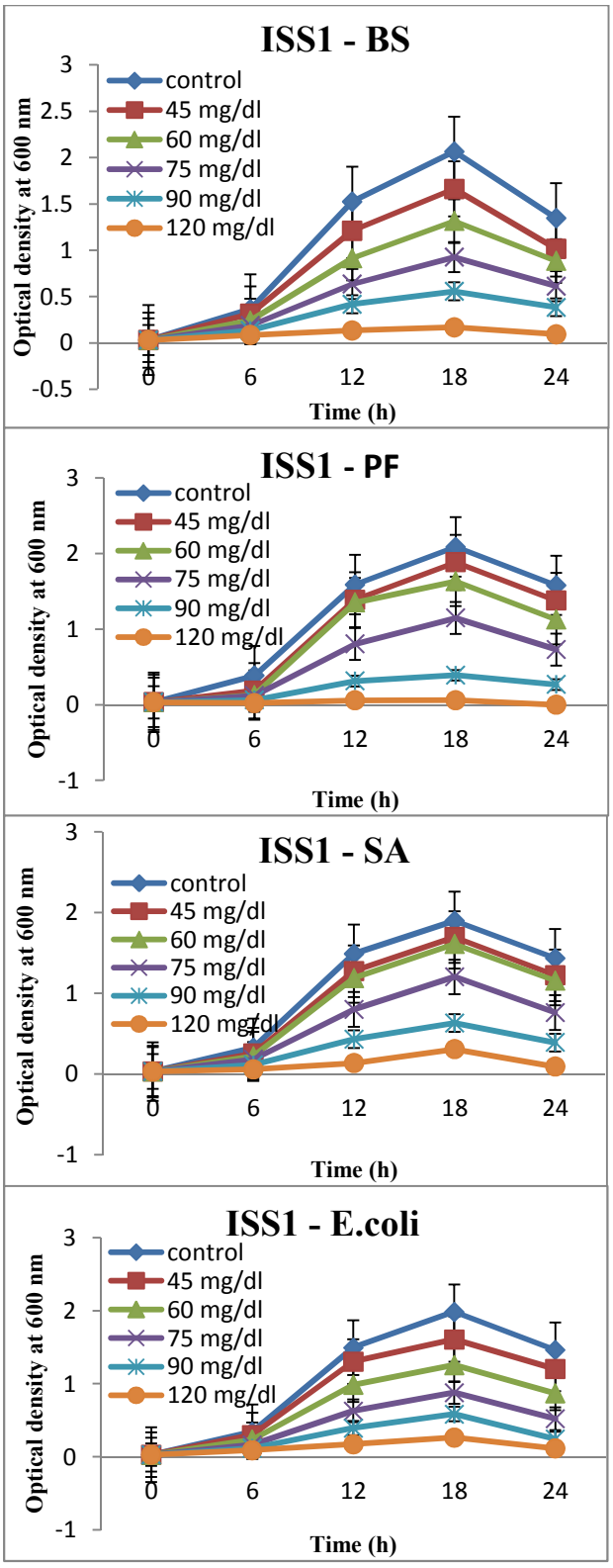

Fig. 9A: Growth curves of bacteria *B. subtilis* (BS), *P. fluorescens* (PF), *S. aureus* (SA) and *E. coli* for the sample ISS1.

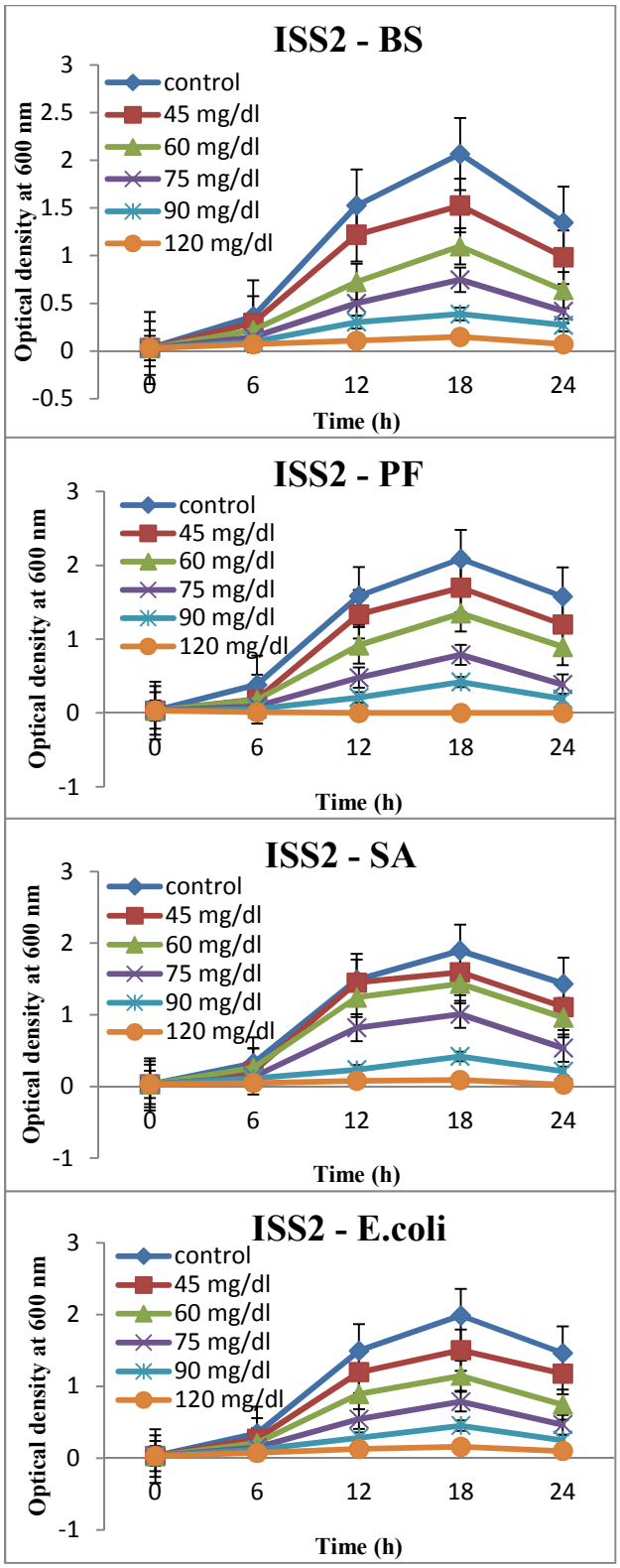

Fig. 9B: Growth curves of bacteria *B. subtilis* (BS), *P. fluorescens* (PF), *S. aureus* (SA) and *E. coli* for the sample ISS2.

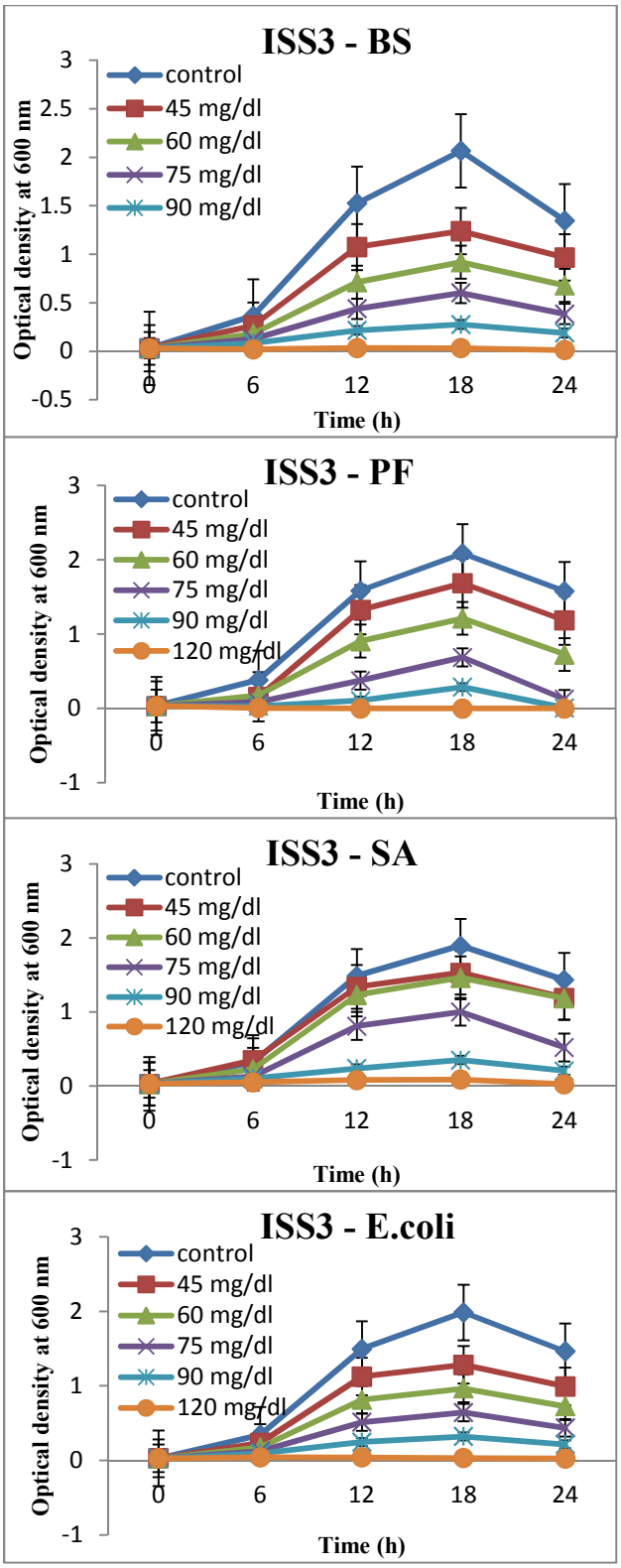

Fig. 9C: Growth curves of bacteria *B. subtilis* (BS), *P. fluorescens* (PF), *S. aureus* (SA) and *E. coli* for the sample ISS3.

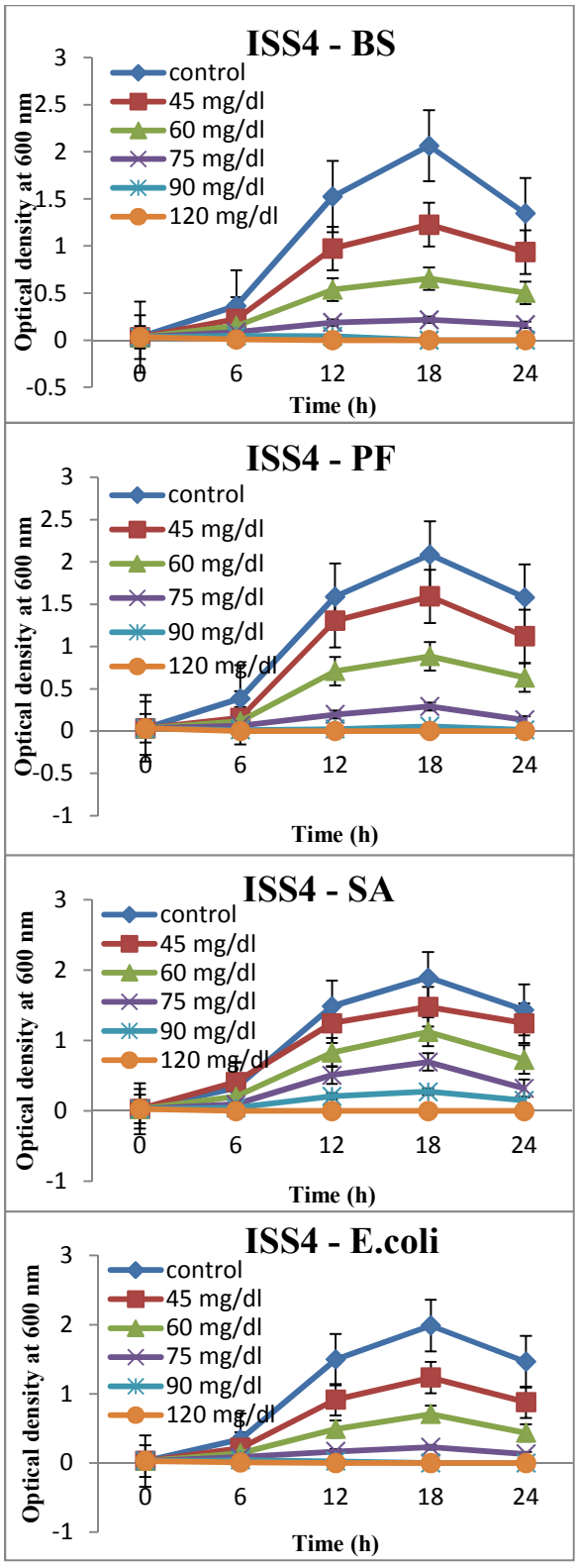

Fig. 9D: Growth curves of bacteria *B. subtilis* (BS), *P. fluorescens* (PF), *S. aureus* (SA) and *E. coli* for the sample ISS4.

Table 4: Inhibition zone size range of undoped and Ag doped α-Fe_2O_3 nanoparticles.

Conc^n of nano particles (in µgs)	Zone of Inhibition (in mm)					
	Bacillus subtilis					
	IS	ISS1	ISS2	ISS3	ISS4	Streptomycin
450	10	10	12	16	19	20
600	10	12	13	17	20	
750	10	13	16	19	20	
	Pseudomonas fluorescens					
450	10	10	10	17	17	19
600	10	11	12	19	20	
750	10	12	13	20	20	
	Staphylococcus aureus					
450	9	10	10	10	10	15
600	9	10	12	14	16	
750	10	11	12	16	16	
	Escherichia coli					
450	9	10	12	13	14	18
600	10	10	13	16	19	
750	10	12	13	19	20	

4. Conclusions

We have successfully fabricated nanostructures of Ag doped α-Fe_2O_3 by using simple, reliable and cost effective chemical route method. The $Fe_{2-x}Ag_xO_3$ nanostructures were characterized by using X-ray diffraction (XRD), Scanning electron microscopy (SEM), Energy dispersive X-ray spectroscopy (EDX), UV Visible spectroscopy, Raman spectroscopy and vibrating sample magnetometer. The antibacterial activity of $Fe_{2-x}Ag_xO_3$ nanostructures were evaluated using inhibition zone and growth curve analysis and are found to be an effective and durable antimicrobial agents, showing enhanced antimicrobial activity due to synergistic effect of Ag^+ ion and native hematite nanostructures.

Acknowledgments

This research was supported by the UGC university research fellowship, Govt. of India. Authors express their thanks to Central Instrumentation Facility Head of Pondicherry University Dr. G. Govindrajan for allowing to characterize our samples through various instruments available at the centre and we are also thankful to the CIF's staff members for their help and co-operation during characterization process.

REFERENCES

1. A. K. Viswanath, Encyclopedia of Nanoscience and Nanotechnology; American Scientific Publishers: Los Angeles, California, USA, 2004.
2. A. K. Viswanath, Handbook of Semiconductor Nanostructures and Nanodevices; American Scientific Publishers: Los Angeles, California, USA, 2006.
3. A. K. Viswanath, Handbook of Surfaces and Interfaces of Materials; Academic Press: 2001.
4. A. K. Viswanath, J. Nanosci. Nanotechnol., 2014, **14,** 1253.
5. A. K. Viswanath, J. Nanosci. Nanotechnol., 2014, **14,** 1947.
6. M. A. Shannon, P. W. Bohn, M. Elimelech, J. G. Georgiadis, B. J. Marinas and A. M. Mayes, Nature, 2008, **452,** 301.
7. K. Fukushima, S. Liu, H. Wu, A. C. Engler, D. J. Coady, H. Maune, J. Pitera, A. Nelson, N. Wiradharma, S. Venkataraman, Y. Huang, W. Fan, J. Y. Ying, Y. Y. Yang and J. L. Hedrick, Nature comm., 2013, **4,** 2861.
8. M. Rai, A. Yadav and A. Gade, Biotechnol. Adv., 2009, **27,** 76.
9. A. Panacek, L. Kvitek, R. Prucek, M. Kolar, R. Vecerova, N. Pizurova, V. K. Sharma, T. Nevecna and R. Zboril, J. Phys. Chem. B., 2006, **110,** 16248.
10. J. R. Nakkala, R. Mata, A. K. Gupta and S. R. Sadras, European Journal of Medicinal Chemistry 2014, **85,** 784.
11. B. Bussa, P. S. Rao, S. Muthukamalam, S. Ramachitra, S. Sudha Rani and T. Swu, Synth. React. Inorg., Met.-Org., Nano-Met. Chem., 2013, **43,** 1073.
12. A. K. Chatterjee, R. Chakraborty and T. Basu, Nanotechnology, 2014, **25,** 135101.
13. R. K. Dutta, B. P. Nenavathu, M. K. Gangishetty and A. V. R. Reddy, Colloids and Surfaces B: Biointerfaces, 2012, **94,** 143.
14. Y. Xie, Y. He, P. L. Irwin, T. Jin and X. Shi, Appl. Environ. Microboil., 2011, **77,** 2325.
15. Z. X. Tang, X. J. Fang, Z. L. Zhang, T. Zhou, X. Y. Zhang and L. E. Shi, Brazilian Journal of Chemical Engineering, 2012, **29,** 775.
16. Q. L. Feng, J. Wu, G. Q. Chen, F. Z. Cui, T. N. Kim and J. O. Kim, Journal of Biomedical Materials Research, 2000, **52,** 662.
17. J. R. Morones, J. L. Elechiguerra, A. Camacho, K. Holt, J. B. Kouri, J. T. Ramirez and M. J. Yacaman, Nanotechnology, 2005, **16,** 2346.
18. T. N. C. Wells, P. Scully, A. E. Proudfoot and M. A. Payton, Biochemistry, 1995, **20,** 7896.
19. V. K. Sharma, R. A. Yngard and Y. Lin, Adv. Colloid Interface Sci., 2009, **145,** 83.

20. X. Li and J. J. Lenhart, Environmental Science & Technology, 2012, **46,** 5378.
21. J. Singh, M. Srivastava, J. Dutta and P. K. Duttaa, Int. J. of Biol. Macromol., 2011, **48,** 170.
22. P. Basnet, G. K. Larsen, R. P. Jadeja, Y. C. Hung and Y. Zhao, ACS Appl. Mater. Interfaces, 2013, **5,** 2085.
23. M. M. Rafi, K. S. Z. Ahmed, K. P. Nazeer, D. S. Kumar and M. Thamilselvan, Appl. Nanosci. DOI 10.1007/s13204-014-0344-z.
24. R. Prucek, J. Tucek, M. Kilianova, A. Panacek, L. Kvitek, J. Filip, M. Kolar, K. Tomankova and R. Zboril, Biomaterials, 2011, **32,** 4704.
25. S. F. Situ and A. C. S. Samia, ACS Appl. Mater. Interfaces, 2014, **6**, 20154.
26. T. Tian, X. Shi, L. Cheng, Y. Luo, Z. Dong, H. Gong, L. Xu, Z. Zhong, R. Peng and Z. Liu, ACS Appl. Mater. Interfaces, 2014, **6,** 8542.
27. S. H. Hu, C. H. Tsai, C. F. Liao, D. M. Liu and S. Y. Chen, Langmuir, 2008, **24,** 11811.
28. X. Mou, Z. Ali, S. Li, and N. He, J. Nanosci. Nanotechnol., 2015, **15,** 54.
29. A. Ito, M. Shinkai, H. Honda and T. Kobayashi, J. Biosci. Bioeng., 2005, **100,** 1.
30. S. G. Grancharov, H. Zeng, S. Sun, S. X. Wang, S. O'Brien, C. B. Murray, J. R. Kirtley and G. A. Held, J. Phys. Chem. B., 2005, **109,** 13030.
31. S. H. Sun, C. B. Murray, D. Weller, L. Folks and A. Moser, Science 2000, **287,** 1989.
32. Y. Tang, Z. Ali, J. Zou, K. Yang, X. Mou, Z. Li, Y. Deng, Z. Lu, C. Ma, M. A. A. Shah, S. Elingarami, H. Yang and N. He, J. Nanosci. Nanotechnol., 2014, **14,** 4886.
33. H. Yang, W. Liang, N. He, Y. Deng and Z. Li, ACS Appl. Mater. Interfaces., 2015, **7,** 774.
34. F. Wang, C. Ma, X. Zeng, C. Li, Y. Deng and N. He, J. Biomed. Nanotechnol., 2012, **8,** 786.
35. H. Yang, Z. Li, Q. Jiang, J. Fan, B. Zhou, Y. Guo, G. Lan, X. Yang, N. He and H. Jiang, J. Nanosci. Nanotechnol., 2015, **15,** 5597.
36. M. Liu, P. Hu, G. Zhang, Y. Zeng, H. Yang, J. Fan, L. Jin, H. Liu, Y. Deng, S. Li, X. Zeng, S. Elingarami and N. He, Theranostics, 2015, **4,** 71.
37. J. Kim, J. E. Lee, J. Lee, Y. Jang, S. W. Kim, K. An, J. H. Yu and T. Hyeon, Angew. Chem., Int. Ed. 2006, **45,** 4789.
38. S. Sacanna and A. P. Philipse, Langmuir, 2006, **22,** 10209.
39. M. Chen, Y. N. Kim, H. M. Lee, C. Li and S. O. Cho, J. Phys. Chem. C., 2008, **112,** 8870.
40. D. Nagao, I. Yokoyama, N. Yamauchi, H. Matsumoto, Y. Kobayashi and M. Konno, Langmuir, 2008, **24,** 9804.
41. S. Maiti, J. Biomed. Nanotechnol., 2011, **7,** 65.
42. Y. Zhang, H. Liu, Y. Jia, Y. Deng, S. Li and N. He, Sci. Adv. Mater., 2015, **7,** 532.
43. Y. Zhang, Y. Jia, S. Li, Y. Deng, H. Liu and N. He, Sci. Adv. Mater., 2014, **6,** 1146.
44. D. K. Yi, S. S. Lee and J. Y. Ying, Chem. Mater., 2006, **18,** 2459.

45. G. Lee, J. Kim and J. H. Lee, Enzyme Microb. Technol., 2008, **42,** 466.

46. J. Ge, H. Lee, L. He, J. Kim, Z. Lu, H. Kim, J. Goebl, S. Kwon and Y. Yin, J. Am. Chem. Soc. 2009, **131,** 15687.

47. J. Ge, L. He, Y. Hu and Y. Yin, Nanoscale, 2011, **3,** 177.

48. H. H. Yang, S. Q. Zhang, X. L. Chen, Z. X. Zhuang, J. G. Xu and X. R. Wang, Anal. Chem., 2004, **76,** 1316.

49. H. Yu, M. Chen, P. M. Rice, S. X. Wang, R. L. White and S. Sun, Nano Lett., 2005, **5,** 379.

50. D. Tang, R. Yuan and Y. Chai, J. Phys. Chem. B., 2006, **110,** 11640.

51. A. W. Bauer, W. M. M. Kirby, J. C. Sherris and M. Turck, Am. J. Clin. Path., 1966, **45,** 493.

52. H. P. Klug, and L. E. Alexander, Wiley InterScience New York, 1954, 504.

53. Y. P. He, Y. M. Miao, C. R. Li, S. Q. Wang, L. Cao, S. S. Xie, G. Z. Yang and B. S. Zou, Phys. Rev. B., 2005, **71,** 125411.

54. D. M. Sherman and T. D. Waite, Am. Miner., 1985, **70,** 1262.

55. L. Chen, X. Yang, J. Chen, J. Liu, H. Wu, H. Zhan, C. Liang and M. Wu, Inorg. Chem., 2010, **49,** 8411.

56. D. Bersani, P. P. Lottici and A. Montenero, J. Raman Spectrosc., 1999, **30,** 355.

57. B. Ahmmad, K. Leonard, M. S. Islam, J. Kurawaki, M. Muruganandham, T. Ohkubo and Y. Kuroda, Advanced Powder Technology, 2013, **24,** 160.

58. H. Ni, Y. Ni, Y. Zhou and J. Hong, Mater. Lett., 2012, **73,** 206.

59. B. B. Straumal, A. A. Mazilkin, S. G. Protasova, A. A. Myatiev, P. B. Straumal, E. Goering, Thin Solid Films 2011, **520,** 1192.